

---

# Princeton Plasma Physics Laboratory

---

PPPL-

PPPL-



Prepared for the U.S. Department of Energy under Contract DE-AC02-09CH11466.

# Princeton Plasma Physics Laboratory

## Report Disclaimers

---

### Full Legal Disclaimer

This report was prepared as an account of work sponsored by an agency of the United States Government. Neither the United States Government nor any agency thereof, nor any of their employees, nor any of their contractors, subcontractors or their employees, makes any warranty, express or implied, or assumes any legal liability or responsibility for the accuracy, completeness, or any third party's use or the results of such use of any information, apparatus, product, or process disclosed, or represents that its use would not infringe privately owned rights. Reference herein to any specific commercial product, process, or service by trade name, trademark, manufacturer, or otherwise, does not necessarily constitute or imply its endorsement, recommendation, or favoring by the United States Government or any agency thereof or its contractors or subcontractors. The views and opinions of authors expressed herein do not necessarily state or reflect those of the United States Government or any agency thereof.

### Trademark Disclaimer

Reference herein to any specific commercial product, process, or service by trade name, trademark, manufacturer, or otherwise, does not necessarily constitute or imply its endorsement, recommendation, or favoring by the United States Government or any agency thereof or its contractors or subcontractors.

---

## PPPL Report Availability

### Princeton Plasma Physics Laboratory:

<http://www.pppl.gov/techreports.cfm>

### Office of Scientific and Technical Information (OSTI):

<http://www.osti.gov/bridge>

---

### Related Links:

[U.S. Department of Energy](#)

[Office of Scientific and Technical Information](#)

[Fusion Links](#)

## Downstream Heat Flux Profile vs. Midplane $T$ Profile in Tokamaks

Robert J. Goldston

Princeton Plasma Physics Laboratory, Princeton NJ 08543

### Abstract

The relationship between the midplane scrape-off-layer electron temperature profile and the parallel heat flux profile at the divertor in tokamaks is investigated. A model is applied which takes into account anisotropic thermal diffusion, in a rectilinear geometry with constant density. Eigenmode analysis is applied to the simplified problem with constant thermal diffusivities. A self-similar nonlinear solution is found for the more realistic problem with anisotropically temperature-dependent thermal diffusivities. Numerical solutions are developed for both cases, with spatially dependent heat flux emerging from the plasma. For both constant and temperature-dependent thermal diffusivities it is found that, below about one-half of its peak, the heat flux profile shape at the divertor, compared with the midplane temperature profile shape, is robustly described by the simplest two-point model. However the physical processes are not those assumed in the simplest two-point model, nor is the numerical coefficient relating  $q_{\parallel div}$  to  $T_{mp} \chi_{\parallel mp} / L_{\parallel}$  as predicted. For realistic parameters the peak in the heat flux, moreover, can be reduced by a factor of two or more from the two-point model scaling which fits the remaining profile. For temperature profiles in the SOL region above the x-point set by marginal stability, the heat flux profile to the divertor can be largely decoupled from the prediction of the two-point model. These results suggest caveats for data interpretation, and possibly favorable outcomes for divertor configurations with extended field lines.

### Introduction

It is of great importance to predict the peak heat flux in ITER and in a future fusion power plant. Unfortunately even reliable empirical scaling results are not available<sup>1</sup>. A range of computational analyses are being applied to this problem, from two-dimensional fluid codes with fixed radial transport coefficients, to turbulence simulations of increasing complexity and fidelity. Here we address a simpler problem but one of importance in interpreting experimental results in this area: If we know the radial profile of the electron temperature in the outer midplane of a tokamak, and we know the divertor magnetic geometry, can we deduce the radial heat flux to its divertor plate, and in particular can we deduce the peak value of that heat flux? This problem is important because reliable measurements are more broadly available of  $T_e(R)$  in the midplane scrape-off layer than of heat flux at the divertor surface, so there is a strong temptation to use these midplane measurements as a proxy for divertor heat flux. Furthermore tokamak designs may be evolving to configurations with relatively greater divertor field line length from the x-point to the divertor surface, and the potential effect of radial thermal diffusion on the peak heat flux in this situation should be understood. We used relatively simple tools in this study to gain physical insight into the relevant effects.

The simplest one dimensional two-point model<sup>2</sup> assumes that each flux tube carries heat from the midplane to the divertor plate independently by Spitzer thermal diffusivity. This model predicts that  $q_{\parallel}$  at the divertor, mapped to the midplane, should vary with R as  $q_{\parallel div} \propto T_{mp} \chi_{\parallel mp} / L_{\parallel} \propto T_{mp}^{7/2}$ , ignoring cross-field thermal diffusion, variations in  $L_{\parallel}$  with  $r$ , volumetric heat losses, ion thermal transport and parallel heat flux reductions due to sheath effects and/or low collisionality. Here we examine solely how cross-field thermal conductivity can make the simplest two-point model

inaccurate by terms of order unity, particularly in the region of peak heat flux. In a purely diffusive model it is the perpendicular thermal conductivity itself that causes the heat spreading that sets both the width of the temperature profile at the midplane and at the divertor. One cannot say *a priori* that these widths will be the same. In particular one expects radial diffusion to play a relatively large role on field lines near the narrow peak of the heat flux, causing a net radial loss of heat between the midplane and divertor.

Here we use a rectilinear-geometry, constant-density thermal diffusion model, ignoring variations in  $L_{\parallel}$ , volumetric heat loss, ion thermal transport, sheaths, and flux limiters. Nonetheless we find that in realistic cases, both in geometry and in thermal diffusivity scaling, the peak heat flux at the divertor plate is lower by a factor in the range of two than would be deduced from assuming heat flux  $\propto T_{mp}^{7/2}$ . Interesting, we also find in the region away from the boundary with the plasma, down roughly a factor of two from the peak heat flux, robust solutions to both the anisotropic heat equation with temperature-independent coefficients and, separately, to the anisotropic heat equation with temperature-dependent coefficients. These solutions do display  $q_{\parallel} \propto T_{mp} \chi_{\parallel mp}$ , although with a proportionality dependent on the temperature scaling of the parallel and perpendicular diffusivity coefficients.

### *Eigenmode Solution*

We start by considering a constant-coefficient thermal diffusion equation, with no sources or sinks within the region under consideration, in order to gain some initial insight. We assume no variation of density across the problem, and no variation in  $L_{\parallel}$ .

Consider then an equation of the form:

$$\frac{\partial}{\partial r} \chi_{\perp} \frac{\partial}{\partial r} T + \frac{\partial}{\partial z} \chi_{\parallel} \frac{\partial}{\partial z} T = 0 \quad (\text{eq. 1})$$

where  $r$  represents the radial distance across the field and  $z$  represents the length along a field line. For now we will consider the thermal diffusivities  $\chi_{\parallel}$  and  $\chi_{\perp}$  both as constants, with

$\chi_{\parallel} \gg \chi_{\perp}$ . Let us consider the solution to be symmetric around  $z = 0$  and to have value 0 at  $z = \pm L_{\parallel}$ . Allow the boundary conditions to be infinitely far away in  $\pm r$ . By separation of variables, we find an eigenfunction solution<sup>3</sup> of the form:

$$T = \sum_n T_n \exp(-r / \lambda_n) \cos[\pi(2n + 1)z / (2L_{\parallel})] \quad (\text{eq. 2})$$

where the eigenvalue,  $\lambda_n$ , is given by:

$$-\chi_{\parallel} \left[ \frac{\pi(2n+1)}{2L_{\parallel}} \right]^2 + \frac{\chi_{\perp}}{\lambda_n^2} = 0; \quad \lambda_n = \pm \sqrt{\frac{\chi_{\perp}}{\chi_{\parallel}}} \frac{2L_{\parallel}}{\pi(2n+1)} \quad (\text{eq. 3})$$

If we consider the region  $r > 0$  and assume that  $T \rightarrow 0$  as  $r \rightarrow \infty$ , we obtain exponential fall-off for all  $n$  by selecting the + sign in equation 3. For  $n = 0$ , this solution is remarkably consistent with the two-point expectation,  $q_{\parallel} \propto T_{mp} \chi_{\parallel mp}$  since  $T(r, z=0)$  and  $q_{\parallel} = \chi_{\parallel} dT/dz|_{z=L_{\parallel}}$  vary together with the exponential scrape-off width  $\lambda_0 = 2L_{\parallel} \sqrt{\chi_{\perp}/\chi_{\parallel}} / \pi$ . However it is interesting to note how this is achieved. If we consider  $r = 0$  to be the boundary between the plasma and scrape-off-layer (SOL), this solution corresponds to a heat flux crossing that boundary which varies as  $\cos[\pi z/(2L_{\parallel})]$ . In other words, the pure  $n = 0$  solution is dependent on the specific cosine heat source profile. Indeed because of this heat flux,  $q_{\parallel}/T$  is  $\pi/2$  greater than would be predicted by the simplest two-point model with all input heat flux at  $z = 0$ . Thus in the case that gives the two-point scaling, individual flux tubes are, at order unity, not carrying heat from the midplane to the divertor independently as is the basis for the simplest two-point analysis.

To gain a sense of the importance of the  $z$ -profile of the cross-boundary heat flux at  $r = 0$ , we take advantage of our linear analysis to consider a range of heat flux profiles to the SOL from the main plasma. We consider the case where there is a constant heat flux,  $q_{\perp,0}$ , across  $r = 0$  between  $z = -L_{\parallel}/\tau$  and  $L_{\parallel}/\tau$ , and zero heat flux across  $r = 0$  outside of this region of  $z$ . This gives us

$$\begin{aligned} q_{\perp}(r=0, z) &= q_{\perp,0} [H(L_{\parallel}/\tau - z) - H(-z - L_{\parallel}/\tau)] \\ &= \frac{\pi(2n+1)\sqrt{\chi_{\perp}\chi_{\parallel}}}{2L} \sum_n T_n \cos[\pi(2n+1)z/(2L_{\parallel})] \end{aligned} \quad (\text{eq. 4})$$

If we multiply both sides by  $\cos[\pi(2n+1)z/(2L_{\parallel})]$  and integrate over  $z$ , we find

$$q_{\perp,0} \int_{-L_{\parallel}/\tau}^{L_{\parallel}/\tau} \cos[\pi(2n+1)\pi z/(2L_{\parallel})] dz = \frac{\pi(2n+1)}{2} \sqrt{\chi_{\perp}\chi_{\parallel}} T_n \quad (\text{eq. 5})$$

giving

$$T_n = \frac{8L_{\parallel}q_{\perp,0}}{\pi^2(2n+1)^2 \sqrt{\chi_{\perp}\chi_{\parallel}}} \sin[\pi(2n+1)/(2\tau)] \quad (\text{eq. 6})$$

Then we have

$$T(z=0, r) = \sum_n T_n \exp(-r/\lambda_n) \quad (\text{eq. 7})$$

and

$$q_{\parallel}(z = L_{\parallel}, r) = \chi_{\parallel} \sum_n (-1)^n T_n \left[ \pi(2n + 1) / (2L_{\parallel}) \right] \exp(-r / \lambda_n) \quad (\text{eq. 8})$$

where  $T_n$  is given by equation 6 and  $\lambda_n$  by equation 3. Note from equation 8 that while the heat flux at the divertor plate for the lowest eigenmode is  $\pi/2$  greater at all radii than would be expected based on the two-point model, when summing over multiple eigenmodes the constancy of this proportionality over radius will not be preserved.

Figure 1 shows  $T(r, z = 0)$  and  $q_{\parallel}(r, z = L_{\parallel})$  for  $\tau = 1.05, 1.2, 2, 5$ . The shapes have been normalized to their values at  $r = 0$ . Also shown is  $2q_{\parallel}(r, z = L_{\parallel})L_{\parallel} / (\pi T(r, z = 0)\chi_{\parallel})$ , which approaches unity as the  $n = 0$  eigenmode dominates. In these calculations 5000 eigenmodes have been included, and the parameters of the diffusion equation and its boundary conditions are:

$$L_{\parallel} = 30m, \quad \chi_{\parallel} = 10^7 m^2 s^{-1}, \quad \chi_{\perp} = 1m^2 s^{-1}.$$

Overall we find the expected result that comes from dimensional analysis: the scale length of the scrape-off width equals, within factors of order unity,  $L_{\parallel} \sqrt{\chi_{\perp} / \chi_{\parallel}} = 9.4\text{mm}$ . Indeed the lowest eigenmode gives 6mm, close to both solutions for  $\tau = 1.2$ . However the upstream and downstream widths also depend significantly on the dimensionless parameter,  $\tau$ . For large values of  $\tau$  (where the heat flux into the SOL is highly localized at the outer midplane) the midplane temperature profile is narrowest, growing for smaller values of  $\tau$ . On the other hand, for large values of  $\tau$  the heat flux at the divertor plate is widest, and for smaller values it is narrowest.

It is clear from the eigenmode analysis that the  $n = 0$  mode should dominate as  $r/\lambda_0$  grows. Indeed we observe in the numerical results that  $q_{\parallel}$  closely approaches the  $n=0$  eigenmode value of  $(\pi/2)T(z=0)\chi_{\parallel}/L_{\parallel}$  away from the effects of the boundary conditions, and so away from the point of peak heat flux. At the peak in the heat flux, we see a strong deviation for the  $n = 0$  and two-point result, upwards by a factor of 1.8 for  $\tau = 1.05$  and downwards to 0.4 for  $\tau = 5$ . The strongest deviation from the  $n = 0$  solution is the region within about a factor of two of the peak heat flux. Away from the region of peak heat flux the simplest 2-point analysis gives a remarkably robust scaling of  $q_{\parallel}$  at the divertor plate with the midplane  $T$ , although not the correct constant of proportionality.

Large values of  $\tau$  might correspond to a physical picture where the heat flux from the core arises from turbulence strongly peaked near the midplane, and where the thermal diffusivity in the SOL is independent of thermal diffusivity in the core. Perhaps the range of the largest values of  $\tau$  can also be considered representative of the Super-X divertor configuration recently proposed<sup>4</sup>.

We conclude from this analysis that in the model under consideration here the relationship between the midplane temperature profile and the heat flux at the divertor plate can agree to within factors of order unity with expectation based on the two-point model, and of the  $n = 0$  eigenmode of the heat equation, but that in the case of a plasma heat source close to the divertor plate ( $\tau = 1.05$ ), and also for cases where the field lines near the divertor are well out of contact with the plasma heat source ( $\tau \geq 2$ ), the radial profile of heat delivered to the divertor plate can be in significant disagreement with such expectation in the important region of peak heat flux.

The insulating boundary condition at  $r = 0$  for  $|z| > L_{||}/\tau$  results in a flat region in  $q_{||}$  close to  $r = 0$ , but, as will be shown below, this is not the cause of the change in shape from the midplane to the divertor surface. In the following analysis we will proceed to solve the thermal diffusion equation numerically, first generalizing the boundary conditions, and then including temperature dependence for both  $\chi_{||}$  and  $\chi_{\perp}$ , to determine what further insight can be derived from a more general diffusive model. The conclusions already reached are confirmed and extended.

### *Finite Difference Solution*

Here we employ a time-forward solution to the thermal diffusivity equation, equation 1, using a simple explicit finite-difference scheme run to equilibrium. As a verification check, this solution was run for the same boundary conditions used in the eigenfunction solution at  $r = 0$ ,  $z = 0$  and  $z = L_{||}$ , and for constant  $d \ln T / dr$  at  $r = 0.04\text{m}$ . For the same diffusion coefficients, the finite-difference approach with 100 zones in the z-direction, and 200 zones in the radial direction, gives agreement with the results shown in figure 1 typically to much better than 1%. The solutions reach their worst-case disagreement of  $\sim 1.5\%$  in  $q_{||}(r) / q_{||}(r=0)$  at  $z = L_{||}$  and  $r \sim 0$ , for the smaller values of  $\tau$ , which place the sharp transition in radial heat flux, which is difficult to resolve with either approach, close to  $z = L_{||}$ .

### *More Realistic Boundary Conditions*

This numerical solution is now generalized to more realistic boundary conditions. For  $z > L_{||}/\tau$ , the boundary condition of zero heat flux at  $r = 0$  is eliminated, and heat is allowed to flow in the negative radial direction across  $r = 0$ . To provide an approximation of the conditions of the private flux region at the region of the x-point, where the outer private flux region meets the inner private flux region, symmetry is assumed for  $r < 0$  across the line  $z = L_{||}/\tau$ . These more general boundary conditions are shown in figure 2.

The results of this analysis, with the above boundary conditions, are shown in figure 3. The calculation reproduces the general behavior seen with the simpler boundary conditions of figure 1, with very similar upstream temperature profiles, but somewhat widened downstream heat flux profiles. The heat flux well away from its peak agrees with the  $n = 0$  eigenmode value of  $(\pi/2)T(z=0)\chi_{||}/L_{||}$  typically to within 0.1%.

In this case the closest agreement in FWHM between the upstream and downstream profile shapes must occur somewhere between  $\tau = 1.05$  and 1.2. Again the dominant effect, except for  $\tau$  close to unity, is the reduction of the peak heat flux due to diffusive losses, and again the effects are concentrated in the region within about a factor of two of the peak heat flux.

Losses into the private flux zone are well known<sup>5</sup>, but the sensitivity of the narrow peak heat flux to diffusive spreading may not receive sufficient emphasis in data analysis. It may be worth noting that the parallel heat flux in the private flux region ( $r < 0$ ), and the reduction of the peak heat flux compared with  $(\pi/2)T(z=0)\chi_{\parallel}/L_{\parallel}$ , can be viewed as a diagnostic of perpendicular diffusion in the divertor leg beyond the plasma, with large diffusion resulting in more nearly symmetric Gaussian-like heat flux patterns reaching into the private flux region, and small diffusion leading to more one-sided exponential shapes. The experimental observation<sup>6</sup> that the peak to average heat flux at the divertor is about a factor of two less than would be deduced from an exponential fit to the heat flux profile is of the same order as this result. Note also that the peak of the heat flux to the divertor shifts significantly outwards from the field line that corresponds to the last closed flux surface, an effect that also should be taken into account in experimental data analysis when attempting to match divertor heat flux patterns with upstream temperature profiles.

### *Temperature-Dependent Thermal Diffusivities - Self-Similarity Solution*

The strong temperature dependence of Spitzer electron thermal diffusivity ( $\chi_{\parallel} \propto T^{5/2}$ ) means that for an isolated flux tube the heat flux to the divertor plate is very strongly sensitive to the upstream temperature. This observation is sometimes used to argue that in the conduction-limited regime the parallel heat flux at the divertor plate should be proportional to  $T^{7/2}$  at the plasma midplane, with insensitivity to other effects such as cross-field diffusion<sup>7</sup>. We want to examine the validity of that argument in a two-dimensional situation. (The reverse argument, not under discussion here, that the upstream temperature should be proportional to  $q_{\parallel}^{2/7}$  is much stronger, because variation in  $q_{\parallel} / [T(z=0)\chi_{\parallel}(z=0)/L_{\parallel}]$  only comes in to the 2/7 power.) In this section we will develop a new solution to the nonlinear heat equation with temperature-dependent thermal diffusivities, based on separation-of-variables and similarity. The final result we find has striking parallels to the  $n = 0$  eigenmode of the linear heat equation.

The anisotropic nonlinear equation we need to solve is:

$$\frac{\partial}{\partial r} \chi_{\perp 0} T^{\alpha} \frac{\partial}{\partial r} T + \frac{\partial}{\partial z} \chi_{\parallel 0} T^{\beta} \frac{\partial}{\partial z} T = 0 \quad (\text{eq. 9})$$

where  $\chi_{\perp 0}$  and  $\chi_{\parallel 0}$  are constants with appropriate dimensions. Interestingly, this nonlinear equation can be analyzed by the separation-of-variables technique, in analogy to the linear heat equation. If we start with the *ansatz*  $T(r, z) = f(r)g(z)$  we can deduce equations for both  $f$  and  $g$ .

$$\left( \frac{\chi_{\perp 0}}{\alpha + 1} \right) \frac{d^2}{dr^2} f^{\alpha+1} = \lambda f^{\beta+1} \quad (\text{eq. 10})$$

and

$$\left( \frac{\chi_{\parallel 0}}{\beta + 1} \right) \frac{d^2}{dz^2} g^{\beta+1} = -\lambda g^{\alpha+1} \quad (\text{eq. 11})$$

where  $\lambda$  is a nonlinear eigenvalue, independent of  $r$  and  $z$ . Note that for the case of  $\alpha = \beta$  we have a generalized version of the linear equation, now with the dependent variable simply  $T^{\alpha+1}$ . Let us consider, however, the equation for  $g(z)$  in the more general case. The boundary conditions for  $g$  are  $dg/dz = 0$  at  $z = 0$ , and  $g = 0$  at  $z = L_{\parallel}$ . For a given value of  $\lambda$ ,  $g(0)$  will adjust to match the boundary condition at  $z = L_{\parallel}$ . The nonlinearity of the problem is reflected in the fact that  $g(0)$  scales as  $\lambda^{1/(\beta-\alpha)}$ , across a self-similar set of solutions with varying  $g(0)$  and  $\lambda$ , all matching the required boundary conditions. Of course for a given solution to the full two-dimensional equation,  $\lambda$  will be constant over  $r$  and  $z$ , so  $g(0)$  will be fixed.

We can gain insight into the solution to equation 11 by numerically computing a single solution,  $h_0(x)$ , for given  $\alpha$  and  $\beta$ , to the closely related Emden-Fowler<sup>8</sup> equation of the form

$$\frac{d^2}{dx^2} h = -h^{(\alpha+1)/(\beta+1)} \quad (\text{eq. 12})$$

with  $h_0(0) = 1$  and  $dh_0/dx = 0$  at  $x = 0$ .  $h_0$  is, evidently, a nonlinear generalization of the cosine function that describes the  $n = 0$  eigenmode of the linear equation. The numerically computed solution to equation 12, shown in figure 5a, first crosses the  $x$ -axis at some distance from the origin,  $d_0$ . Then if we set

$$\lambda = \lambda_0 = \frac{\chi_{\parallel 0}}{(\beta + 1)} \left( \frac{d_0}{L_{\parallel}} \right)^2 \quad (\text{eq. 13})$$

in equation 11 and substitute  $z = xL_{\parallel}/d_0$ , we find that  $g_0(z) = h_0^{1/(\beta+1)}(zd_0/L_{\parallel})$  is the solution to equation 11, with  $g(0) = 1$ . The more general solution, allowing non-unity  $g(0)$  is

$$g(z) = g(0)h_0^{1/(\beta+1)}(zd_0/L_{\parallel}); \quad \lambda = \lambda_0 g^{(\beta-\alpha)}(0) \quad (\text{eq. 14})$$

Since  $T^{\beta+1}(z) \propto g^{\beta+1}(z) \propto h_0(zd_0 / L_{\parallel})$ , the heat flux at the divertor plate, for all  $r$ , is given by

$$-\chi_{\parallel 0} T^{\beta} \frac{\partial T}{\partial z} \Big|_{z=L_{\parallel}} = -\frac{\chi_{\parallel 0}}{\beta+1} \frac{\partial T^{\beta+1}}{\partial z} \Big|_{z=L_{\parallel}} = -T^{\beta+1}(z=0) \frac{\chi_{\parallel 0}}{(\beta+1)L_{\parallel}} d_0 \frac{dh_0}{dx} \Big|_{x=d_0} \quad (\text{eq. 15})$$

This equation indicates that in regions of the plasma where the separation-of-variables *ansatz* holds, the heat flux will scale radially as  $T(r, z=0)^{\beta+1}$ , since all the other factors are independent of  $r$ . Remarkably, this result is equal to that of the simple two-point model (with all heat flux originating at  $z = 0$ ), multiplied by the factor  $d_0 (dh_0/dx)|_{x=d_0}$ . We can easily calculate  $d_0$  and  $d_0 (dh_0/dx)|_{x=d_0}$  numerically as a function of  $(\alpha + 1)/(\beta + 1)$ , as shown in figure 4. The result is in good agreement with analytic solutions for the cases of  $(\alpha + 1)/(\beta + 1) = 0, 1$  and  $\infty$ , giving for  $d_0 (dh_0/dx)|_{x=d_0} = 2, \pi/2$ , and 1, respectively. The two extreme cases correspond to heat deposition independent of  $z$ , and heat deposition localized at  $z = 0$ , which have been analyzed previously<sup>9</sup>. The middle case corresponds to the  $n = 0$  eigenmode of the linear problem discussed here. Some cases of interest are listed in Table 1.

$(\alpha + 1)/(\beta + 1)$	$d_0 (dh_0/dx) _{x=d_0}$	Comment
0	2.0	Heat source independent of $z$ .
2/7	1.821	Spitzer parallel, constant perpendicular.
4/7	1.698	Spitzer parallel, Bohm perpendicular.
1	$1.571 = \pi/2$	$n = 0$ eigenmode of linear problem, and $\alpha = \beta$ .
1.5	1.472	
2	1.402	
$\infty$	1.0	Heat source at $z = 0$ . Simple two-point model.

TABLE 1. Normalized heat flux vs. temperature dependence of thermal diffusivities, for self-similar nonlinear solution.

Equation 10, the radial equation, is also interesting. The equation we need to solve to provide a self-similar solution for  $f(r)$  is also an Emden-Fowler<sup>7</sup> equation, of the form

$$\frac{d^2}{dx^2} k = k^{(\beta+1)/(\alpha+1)} \quad (\text{eq. 16})$$

Let us define  $k_0(x)$  as the solution to equation 16 for which  $k(0) = 1$ , and for which the limit of  $k$  as  $x$  goes to infinity is 0. This uniquely determines  $dk/dx$  at  $x = 0$  and so  $k_0$  as a function of  $(\beta + 1)/(\alpha + 1)$ . Solutions with  $k < 0$  for any  $x > 0$  are unphysical; solutions with  $dk/dx > 0$  for any  $x > 0$  correspond to a physical situation with a second heat source at finite  $r$ .  $k_0$  is, evidently, a nonlinear generalization of the exponential function that appears in the  $n = 0$  eigenmode of the linear equation.  $k_0(x)$  for given  $(\beta + 1)/(\alpha + 1)$  and relevant for our physical situation can be readily computed numerically using a shooting method, with results shown in figure 5b.

We can easily see that

$$f_0(r) = k_0^{1/(\alpha+1)} \left( \left( \frac{\alpha+1}{\chi_{\perp 0}} \lambda \right)^{1/2} r \right) \quad (\text{eq. 17})$$

is a solution to equation 10 with  $f_0(0) = 1$ . A more general solution, allowing non-unity  $f(0)$  is

$$f(r) = f(0) k_0^{1/(\alpha+1)} \left( \left( \frac{\alpha+1}{\chi_{\perp 0}} \lambda_0 g^{(\beta-\alpha)}(0) f^{(\beta-\alpha)}(0) \right)^{1/2} r \right) \quad (\text{eq. 18})$$

where we have used equation 14 to substitute for  $\lambda$  in terms of  $\lambda_0$  and  $g(0)$ . Let us assume that at some position  $r = 0$  and  $z = 0$ , we know  $T = T_0 = f(0)g(0)$ . Then the final result is

$$T(r, z) = T_0 k_0^{1/(\alpha+1)} \left( \left( \frac{\chi_{\parallel 0} T_0^\beta / (\beta + 1)}{\chi_{\perp 0} T_0^\alpha / (\alpha + 1)} \right)^{1/2} \frac{d_0}{L_{\parallel}} r \right) h_0^{1/(\beta+1)} \left( \frac{d_0}{L_{\parallel}} z \right) \quad (\text{eq. 19})$$

This solution to the nonlinear anisotropic heat equation has a structure that is strikingly similar to that of the  $n = 0$  eigenmode, equations 2 and 3, which is of course one solution of the linear heat equation.  $k_0$  generalizes the exponential, and  $h_0$  the cosine. The scaling of the ratio of the radial scale length to the parallel scale length with the square root of the ratio of the perpendicular to parallel thermal diffusivity is preserved. For the case of  $\alpha = \beta$  equation 19 reduces to the  $n = 0$  eigenmode of the linear equation for  $T^{(\alpha+1)}$  and for  $\alpha = \beta = 0$  to the  $n = 0$  eigenmode of the linear equation for  $T$ .

Returning to figure 5, we see  $k_0$  and  $h_0$  for a number of the cases listed in table 1. While  $h_0$  is relatively unremarkable,  $k_0$  has the physically intuitive feature that for  $\alpha > \beta$  the radial gradient scale length becomes shorter with increasing  $r$ , and for  $\beta > \alpha$  the gradient scale length increases. For example, for Spitzer thermal diffusivity, with relatively large  $\beta = 5/2$ , one expects that the parallel loss time will grow as  $T$  falls with  $r$ , giving relatively more time for radial diffusion (so long as  $\alpha < \beta$ ), and so greater radial scale length.

Just like the  $n = 0$  eigenmode solution to the anisotropic linear equation, this is not the only solution to the anisotropic nonlinear equation, but it should dominate away from special boundary conditions. Thus we expect a numerical solution to converge to equation 19, appropriately translated in  $r$  and/or reflected to  $-r$ , away from the region of peak heat flux, where the effects of boundary conditions (including between  $+r$  and  $-r$  solutions) are strongest.

### *Temperature-Dependent Thermal Diffusivities - Numerical Results*

To include the effects of specific boundary conditions, the heat diffusion equation was solved in the general geometry of figure 2, taking a Spitzer-like  $\chi_{\parallel} = 10^7 T^{5/2} \text{ m}^2 / \text{sec}$  and a Bohm-like

$\chi_{\perp} = T \text{ m}^2 / \text{sec}$ . The input heat flux was adjusted to set the maximum of  $T$  to 1.0 for all cases. In dimensional units, for Spitzer thermal diffusivity  $T = 1$  corresponds to  $T_e = 50 \text{ eV}$ ,  $n_e = 10^{19}/\text{m}^3$  and  $Z_{eff} = 2$ . For Bohm thermal diffusivity,  $T = 1$  corresponds  $T_e = 50 \text{ eV}$  and  $B = 3\text{T}$ .

The numerical convergence of the thermal diffusion equation to equilibrium, with strongly temperature-dependent thermal diffusivities, is slower than for the constant-diffusivities equation, since the Courant condition on the time step in the hottest regions is unchanged, but the thermal diffusivity in the lower temperature regions is significantly reduced. To adjust for this, Jacobi iteration is employed in which the iteration “time” step is scaled locally by  $1/T(r, z, t)$  relative to the simple diffusion equation. Iterations continue until convergence is established.

The numerical results using temperature-dependent thermal diffusivity coefficients, and using the boundaries shown in figure 2, are shown in figure 6. Radially away from the plasma heat source that forces the solution away from a self-similar  $z$  dependence, and therefore away from the peak heat flux, about one-half way below the peak value,  $q_{\parallel}$  approaches  $1.698 (2/7)T(z=0)\chi_{\parallel}(z=0)/L_{\parallel} = 0.485 T(z=0)\chi_{\parallel}(z=0)/L_{\parallel}$ , as predicted in equation 15, based on the nonlinear similarity solution. Ultimately it matches this value to  $\sim 0.1\%$  accuracy. Furthermore, as shown in figure 7, away from  $r = 0$   $T(r, z)$  is found to be in quite good agreement with the self-similarity solution with  $T_0 = 1$  at  $r = z = 0$ . Close to  $r = 0$ , however, distortion away from self-similarity due to the boundary condition is clearly visible.

Overall, the results shown in figure 6 are qualitatively similar to those with constant coefficients, but the degree of downstream radial spreading relative to the upstream temperature profile is increased, again largely because of reduction in the peak heat flux. The best fit between the upstream  $T\chi_{\parallel}$  and  $q_{\parallel}$  at the divertor plate is achieved in this case for the relatively extreme  $\tau = 1.05$ . This can be understood by noting that as the temperature decreases along the field lines towards the divertor plate, Spitzer parallel diffusivity is reduced more strongly than Bohm perpendicular diffusivity, giving the radial spreading a relatively larger role.

Figure 8 shows equivalent calculations for what might be considered the most conventional case of constant  $\chi_{\perp} = 1m^2 / sec$  and parallel thermal conductivity scaling as  $T^{5/2}$ . (Here Jacobi iteration is not possible, so much longer runs are required to achieve convergence.) The divertor heat flux profile is wider yet, consistent with the hypothesis that decreased parallel diffusivity at low  $T$  allows a larger relative role for perpendicular diffusivity. Again, following the rule of thumb from earlier calculations, in the region where the heat flux drops below about one-half of its peak value, the scaling is dominated by the expected two-point scaling including the numerical constant defined by the nonlinear solution, in this case  $0.520 = (2/7) 1.821$ .  $\tau = 1.2$  and constant perpendicular diffusivity might be considered the most “realistic” case analyzed here. Note that for these conditions the  $q_{\parallel}$  profile maps to about three times the FWHM of  $T^{7/2}$  at the midplane. The peak heat flux is reduced by a factor of more than two from the two-point model applied with the numerical coefficient from the nonlinear solution.

This analysis, by construction, does not include variation in the plasma density, and one can note that the effect seen here would be further enhanced if pressure balance were maintained along each flux tube. Under such circumstances the density increases as a field line approaches the divertor plate and the temperature falls. The parallel heat flux due to Spitzer conductivity is not affected by the change in density, only by the reduction in temperature. However in the general case for radial diffusion, and for Bohm diffusion in particular, one expects the radial heat flux to increase with density, therefore increasing the broadening of the heat flux distribution, particularly in the region close to the divertor surface, relative to the model examined here. Along with volumetric power losses, this may contribute to the reduction in peak heat flux observed as the density is increased in tokamaks.

One might be inclined to reduce  $\alpha$  by unity, to account for the effect of increasing density with decreasing temperature along a field line, but while the parallel density profile, for fixed pressure, would be handled appropriately, the resulting effective cross-field density profile would be inappropriate. Studies with varying density are left to investigations with larger codes.

#### *Fixed Temperature Profile in Plasma-Attached SOL*

The analyses to this point have assumed identical parallel and cross-field thermal transport coefficients in the region of the SOL in contact with the plasma as in the divertor leg away from the LCFS (in the more general geometry case). It is interesting to consider an alternate scenario, in which the SOL region in contact with the plasma has a profile set by a marginal stability condition. The heat flux from the plasma is assumed to adjust to sustain this particular profile. An analysis of experimental electron temperature measurements in the plasma edge and near-SOL region<sup>10</sup> suggests that this characteristic SOL width, in the outer midplane, scales with plasma major radius, and not with other parameters such as SOL power, magnetic field, or plasma current, in contrast with observations of heat flux at the divertor plate<sup>11,6,12,13,14</sup>. One can ask whether under these conditions the heat flux to the divertor plate is necessarily tied to the SOL temperature profile in contact with the plasma.

To investigate this problem the model considered above, with Spitzer-like parallel thermal conduction and constant perpendicular thermal conduction is used, but now with the temperature profile in the whole region contiguous with the plasma ( $z < L_{||}/\tau$ ) taken to be of the form:

$T = 0.9e^{-r/\lambda} + 0.10$ , where the latter term represents, for example, a 5 eV far SOL region in the case of a 50 eV LCFS temperature. To consider a likely extreme case where this condition of marginal stability is strictly imposed along two-thirds of the field line length, we take  $\tau = 1.5$ . In figure 8a we show  $T^{7/2}$  at the midplane and  $q_{||}$  at the divertor plate, for the same physical model as used in figure 8. Indeed figure 9a can be viewed as an additional member of the set of figures 8a-d. In figures 9b-d  $T$  is held constant for  $|z| < L_{||}/\tau$ , with  $\lambda = 1, 2$  and 4cm. Comparison of  $q_{||}/(T_{mp}^{7/2}\chi_{||0}/L_{||})$  with the self-similarity solution is not really appropriate, since the boundary condition for this case is set at  $z = 0$ , placing it squarely in the solution region of interest. In the plots, however, this comparison is made, taking  $L_{||} = 10m$ . In this case even away from the region of peak heat flux the simple two-point scaling does not pertain.

Eliminating diffusion along two-thirds of the SOL field line results in a somewhat reduced width at the divertor plate, but that width is only moderately sensitive to the width of the temperature profile in the vicinity of the plasma. A factor of four change in the profile width contiguous to the plasma results in a factor of 1.6 change in the heat flux FWHM at the divertor plate. Figure 10 shows contours of  $T$  for the cases shown in figure 9. There is no diffusion of heat in the negative  $z$  direction that could interfere with the ability of the plasma to set a narrow width in the SOL near the plasma, except around 2cm and beyond in the lowest  $\lambda = 1cm$  case. Thus return heat flux would have little impact on the ability of the plasma to sustain itself near marginal stability over two e-folds. In sum, in this case the heat flux profile to the divertor and midplane electron temperature profile are largely decoupled, even in the region below half of the peak heat flux.

### *No Radial Diffusion in Divertor Leg*

We also examined the reverse of the above model, meant to simulate a situation where the thermal diffusion in the SOL is driven exclusively by the turbulence at the edge of the bulk plasma, concentrated near the midplane, with no radial diffusion beyond the x-point. In this case we looked at  $\tau = 2$ , Spitzer parallel thermal diffusivity, constant  $1 m^2/sec$  perpendicular thermal diffusivity in the region  $|z| < L_{||}/\tau$ , and zero perpendicular diffusivity for  $|z| > L_{||}/\tau$ . This gave a drop in  $T$ , but very little change in the  $T(r)$  profile between  $z = 0$  and  $|z| = L_{||}/\tau$ . The calculated heat flux to the divertor plate was equal to  $(2/7) \chi_{||0} T^{7/2}(r, z = L_{||}/\tau)/(L_{||}(1-1/\tau))$ , providing another verification check on the solution to the equation with non-constant coefficients. This calculation shows that if the assumptions of the two-point model are enforced, the result is as expected. If there is little perpendicular diffusion away from the region close to the midplane, and the midplane is where most of the heat is deposited into the SOL, then one can indeed expect the heat flux to the divertor plate to vary as  $T^{7/2}$  at the midplane, even with the expected coefficient of proportionality. On the other hand, parallel connection along field lines suggests that

turbulent  $ExB$  driven diffusion in the SOL would be distributed along its length. Indeed strong turbulence is observed in the SOL far from the midplane<sup>15</sup>, as well as on Langmuir probes in divertor plates<sup>16</sup>.

### *Conclusions*

One conclusion from these studies is that one should not expect the parallel heat flux profile to the divertor plate to vary as  $T_{mp}^{7/2}$  in the region of peak heat flux, as might have been thought from a simple two-point model of conduction-limited thermal transport with Spitzer electron thermal conductivity. The level of radial diffusion that induces the mid-plane temperature profile width also broadens the heat flux along the field lines leading to the divertor plate, even without additional physical effects such as radiation or detachment, nor density increase near the divertor. The peak in the heat flux can be significantly reduced and can shift outwards from the separatrix field line. On the other hand, away from the peak in the heat flux for both the linear and nonlinear versions of the heat equation examined here, the result that  $q_{\parallel div} \propto T_{mp} \chi_{\parallel mp} / L_{\parallel}$ , which varies as  $T_{mp}^{7/2}$  for Spitzer parallel thermal diffusivity, is remarkably robust although not driven by the physics of exclusively parallel heat flux. The constant of proportionality varies depending on the temperature scaling of the diffusivities. This proportionality does not hold, however, in the case where the midplane temperature profile is set, for example, by a marginal stability condition. In this case the midplane temperature profile and divertor heat flux profile are largely decoupled.

An encouraging conclusion from this analysis is that if there is radial thermal diffusion along the field lines distant from the midplane, concepts such as the X-divertor<sup>17</sup>, Snowflake divertor<sup>18</sup> and particularly Super-X divertor<sup>4</sup> may offer an enhanced opportunity for thermal diffusion to contribute to heat flux dispersion, as a complement to the magnetic flux expansion central to these designs.

It is important to note that we need to be cautious in applying a purely diffusive model such as this for thermal perpendicular transport in the SOL. The assumption of constant density is a significant limitation in this study. Also at high density volumetric power losses play an important role. Longer field lines just near the separatrix, not taken into account here, may reduce parallel losses. Flux limitations due to sheath effects and low collisionality may play an important role at low density. This class of study should be revisited using more complete codes to include such effects.

Since the measured transport coefficients are in the range of Bohm, and since one observes large-scale convective density perturbations, so-called “blobs”, in the edge<sup>19</sup>, it could be that heat is significantly transferred to the SOL from the main plasma in large convective events, and drained out along (and across) field lines. This is consistent with the order unity fluctuations measured in SOL parameters<sup>20</sup>. This might also be consistent with the observation that the edge and SOL electron temperature gradient scale length in the outer midplane is observed to vary

with system size, suggesting a role for marginal stability in setting that scale length. The analysis here suggests that if the mid-plane scale length is set by a marginal stability criterion and sand-pile-like intermittent response, the peak heat flux profile at the divertor plate should not be expected to vary as the midplane profile of  $\langle T_e \rangle^{7/2}$ .

### *Acknowledgments*

The author thanks Dr. S. Jardin for a helpful discussion of Jacobi iteration, Dr. W. Fundamenski for valuable discussions of the role of intermittency in SOL physics, Dr. P. Stangeby for very valuable discussions of how to interpret these results and Dr. T. Rognlein for useful discussions of the full 2-d models. This work supported by U.S. DOE Contract # DE-AC02-09CH11

---

<sup>1</sup> Loarte, A., *et al.*, “Progress in the ITER Physics Basis, Chapter 4: Power and Particle Control”, Nuclear Fusion 47 (2007) p. S203 – S263

<sup>2</sup> Stangeby, P.C., “The Plasma Boundary of Magnetic Devices”, Taylor and Francis Group, New York, 2000, p. 226, eq. 5.7

<sup>3</sup> Carslaw, H.S. and Jaeger, J.C., “Conduction of Heat in Solids”, Oxford University Press, London, 1959, p. 163 and *ff.*

<sup>4</sup> Valanju, P.M., *et al.*, “Super-X Divertors and High Power Density Fusion Devices”, Physics of Plasmas 16 (2009) p. 056110

<sup>5</sup> Harrison, M.F.A., and Hotson, “Edge plasma and surface conditions in ITER”, E.S., Journal of Nuclear Materials 176 & 177 (1990) p. 256

<sup>6</sup> Loarte, A., *et al.*, “Multi-machine Scaling of the Divertor Peak Heat Flux and Width for L-mode and H-mode Discharges”, Journal of Nuclear Materials 266 (1999) pgs. 587-592

<sup>7</sup> Ahn, J.-W., *et al.*, “The Role of Parallel Heat Transport in the Relation Between Upstream Scrape-off Layer Widths and Target Heat Flux Width in H-mode Plasmas of the National Spherical Torus Experiment”, Physics of Plasmas 15 (2008) pgs. 122507 1–8

<sup>8</sup> Handbook of Exact Solutions for Ordinary Differential Equations, A.D. Polyanin, V. F. Zaitsev, CRC Press, Boca Raton, 1995

<sup>9</sup> Stangeby, P.C., *Op. Cit.*, p. 187 and *ff.*

<sup>10</sup> Kallenbach, A., *et al.*, “Multi-machine Comparisons of H-mode Separatrix Densities and Edge Profile Behavior in the ITPA SOL and Divertor Physics Topical Group”, Journal of Nuclear Materials 337-339 (2005) pgs. 381 – 385

<sup>11</sup> Lipschultz, B, private communication, 2009

- <sup>12</sup> Counsell, G.F., *et al.*, “SOL Width Scaling from Consideration of Edge Transport in Tokamaks”, *Journal of Nuclear Materials* 266-269 (1999) pgs. 91 –98
- <sup>13</sup> Fundamenski, W., *et al.*, “Boundary Plasma Energy Transport in JET ELMy H-Modes”, *Nuclear Fusion* 44 (2004) pgs. 20 - 32
- <sup>14</sup> Ahn, J.W. *et al.*, “Dependence of SOL Widths on Plasma Current and Density in NSTX H-mode Plasmas”, *Journal of Nuclear Materials* 390-391 (2009) pgs. 421-424
- <sup>15</sup> Terry, J.L., *et al.*, “Spatial Structure of Scrape-off Layer Filaments Near the Midplane and X-point Regions of Alcator C-Mod”, *Journal of Nuclear Materials* 390-391 (2009) pgs. 339-342
- <sup>16</sup> Garcia-Cortes, I., *et al.*, “Characterization of Fluctuations in the JET Divertor Plasmas with Langmuir Probes”, *Plasma Physics and Controlled Fusion* 38 (1996) 2051-2062
- <sup>17</sup> Kotschenreuther, M., *et al.*, “On Heat Loading, Novel Divertors, and Fusion Reactors”, *Physics of Plasmas*, 14 (2007) p. 072502
- <sup>18</sup> Umansky, M.V., *et al.*, “Analysis of Geometric Variations in High-Power Tokamak Divertors”, *Nuclear Fusion* 49 (2009) p. 075005
- <sup>19</sup> Zweben, S., *et al.*, “Edge Turbulence Measurements in Toroidal Fusion Devices”, *Plasma Physics and Controlled Fusion* 49 (2007) Pgs. S1-S23
- <sup>20</sup> Boedo, J.A., “Edge Turbulence and SOL Transport in Tokamaks”, *Journal of Nuclear Materials* 390-391 (2009) pgs. 29 – 37

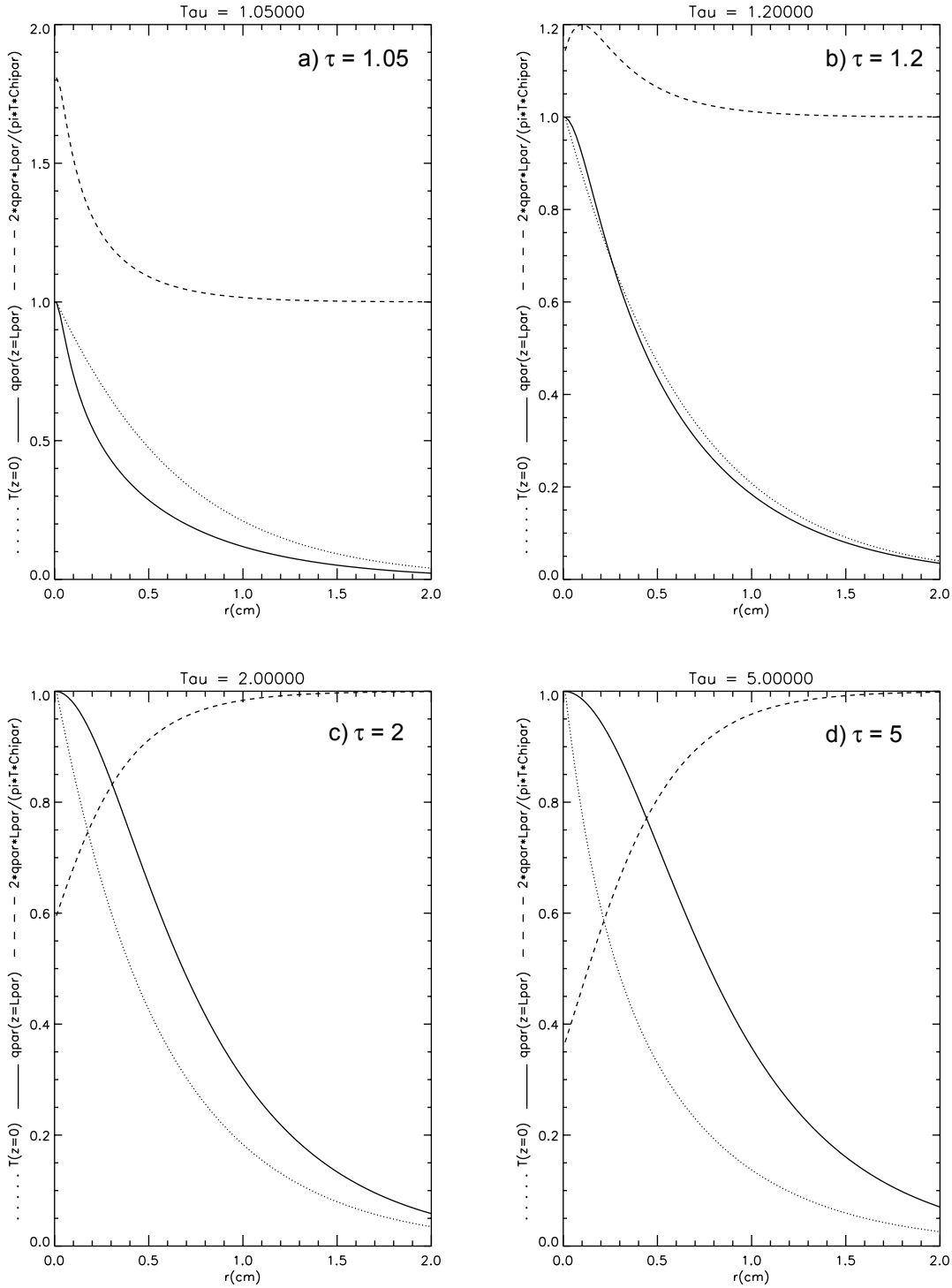


**Figure 1:**  $T(r)$  at  $z = 0$ ,  $q_{||}(r)$  at  $z = L_{||}$  and  $2q_{||}(r, z = L_{||})L_{||} / (\pi T(r, z = 0)\chi_{||})$  for various values of  $\tau$ , based on eigenmode expansion for constant thermal diffusivities and simplest boundary conditions.

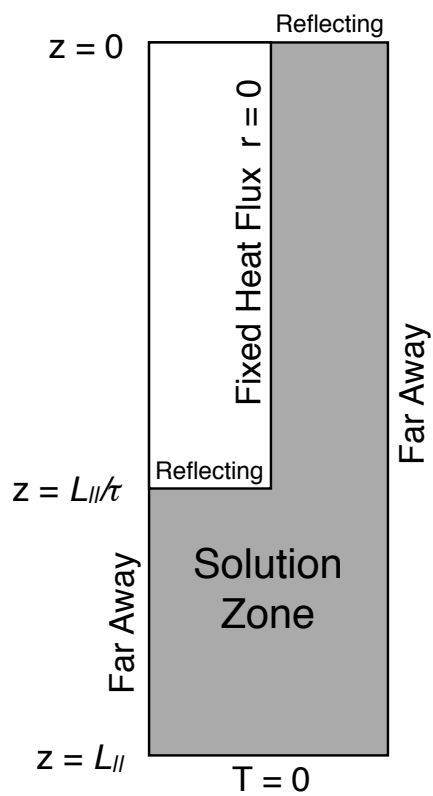


**Figure 2:** More realistic boundary conditions used in subsequent analyses. At the “far away” boundaries  $d \ln T / dr$  is set constant. Convergence studies are used to adjust the outer limit of the calculation.

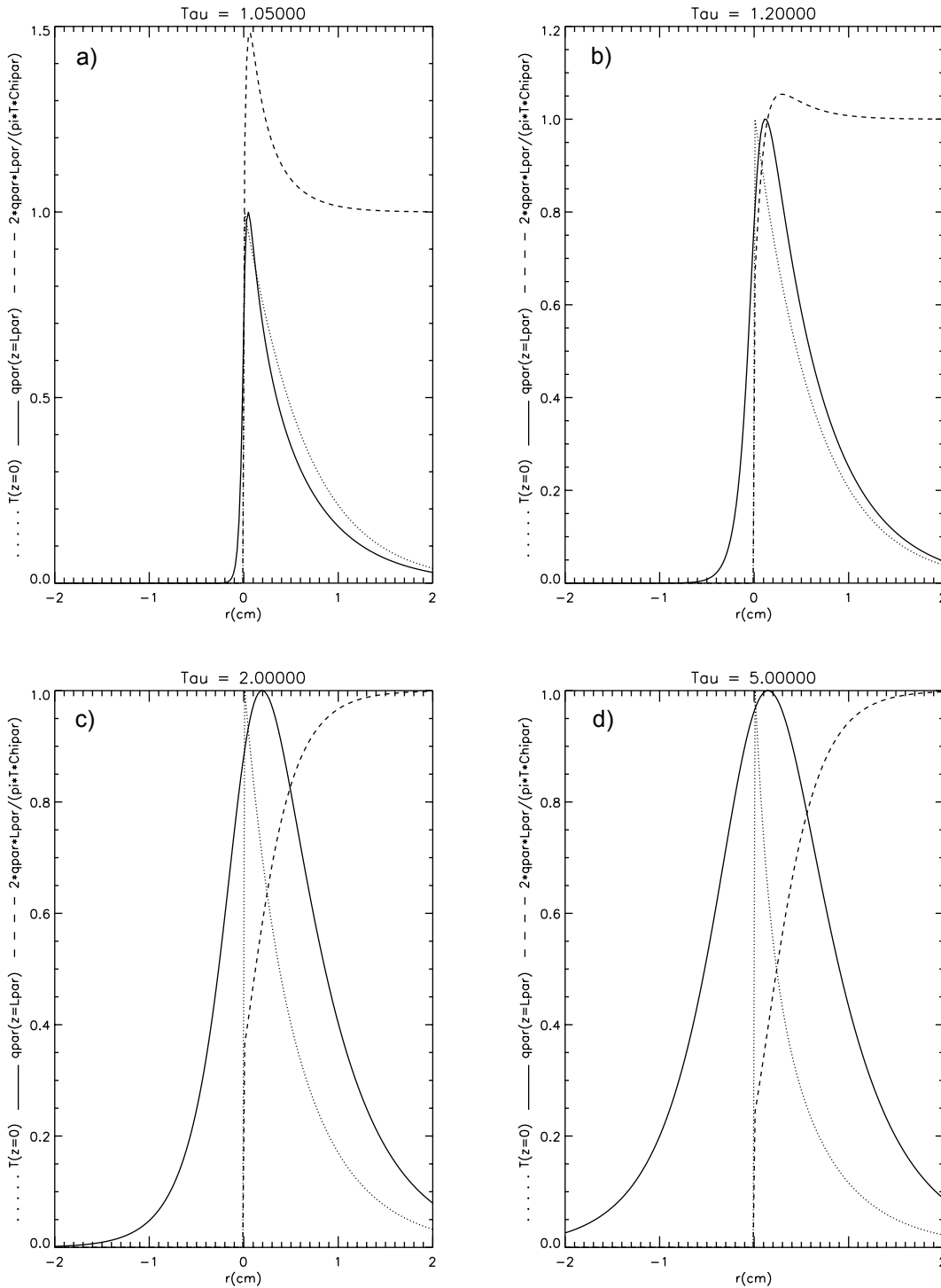


**Figure 3.**  $T(r)$  at  $z = 0$ ,  $q_{\parallel}(r)$  at  $z = L_{\parallel}$  and  $2q_{\parallel}(r, z = L_{\parallel})L_{\parallel} / (\pi T(r, z = 0)\chi_{\parallel})$ , ratio of divertor heat flux to midplane

$T$  normalized to expectation based on  $n = 0$  eigenmode, for various values of  $\tau$ . Numerical solution with constant thermal diffusivities and boundary conditions of figure 2.

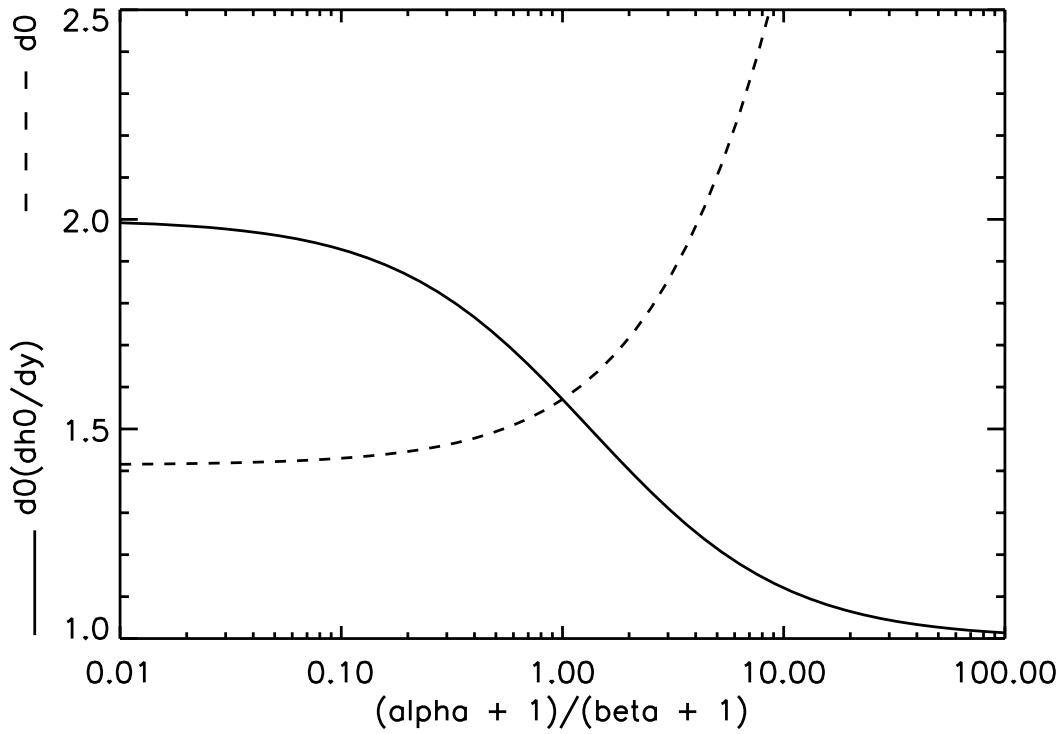


**Figure 4.** Heat flux relative to the simple two-point model  $d_0(dh_0/dy)$  and dimensionless scale length  $d_0$  vs. temperature coefficients of thermal diffusivities.

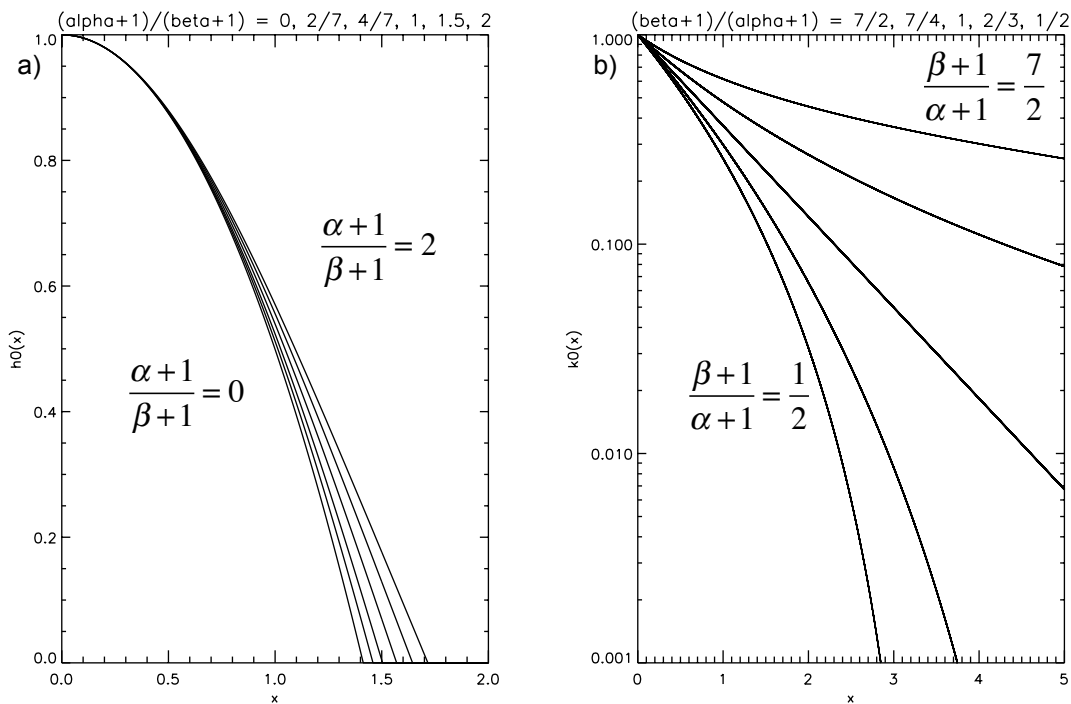


**Figure 5.** Profiles of  $h_0$  and  $k_0$  for various values of  $(\alpha + 1)/(\beta + 1)$ .

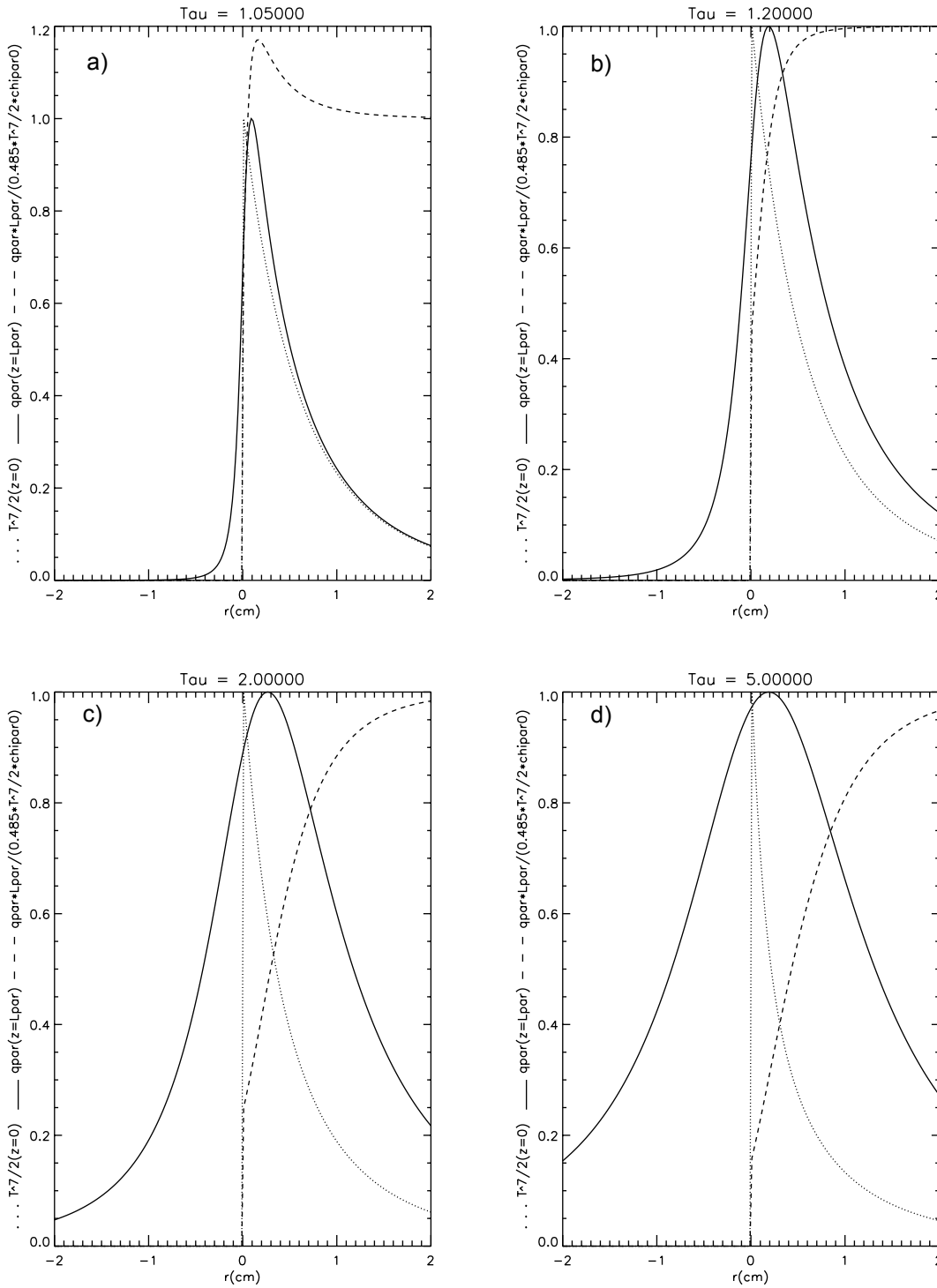


**Figure 6.**  $T^{7/2}(r)$  at  $z = 0$ ,  $q_{\parallel}(r)$  at  $z = L_{\parallel}$  and  $q_{\parallel}(r, z = L_{\parallel})L_{\parallel} / (0.485T^{7/2}(r, z = 0)\chi_{\parallel 0})$ , ratio of divertor heat flux to midplane  $T^{7/2}$  normalized to expectation based on self-similarity solution, for various values of  $\tau$ . Numerical solution with Spitzer scaling of parallel thermal diffusivity, Bohm scaling of perpendicular, and boundary conditions of figure 2.

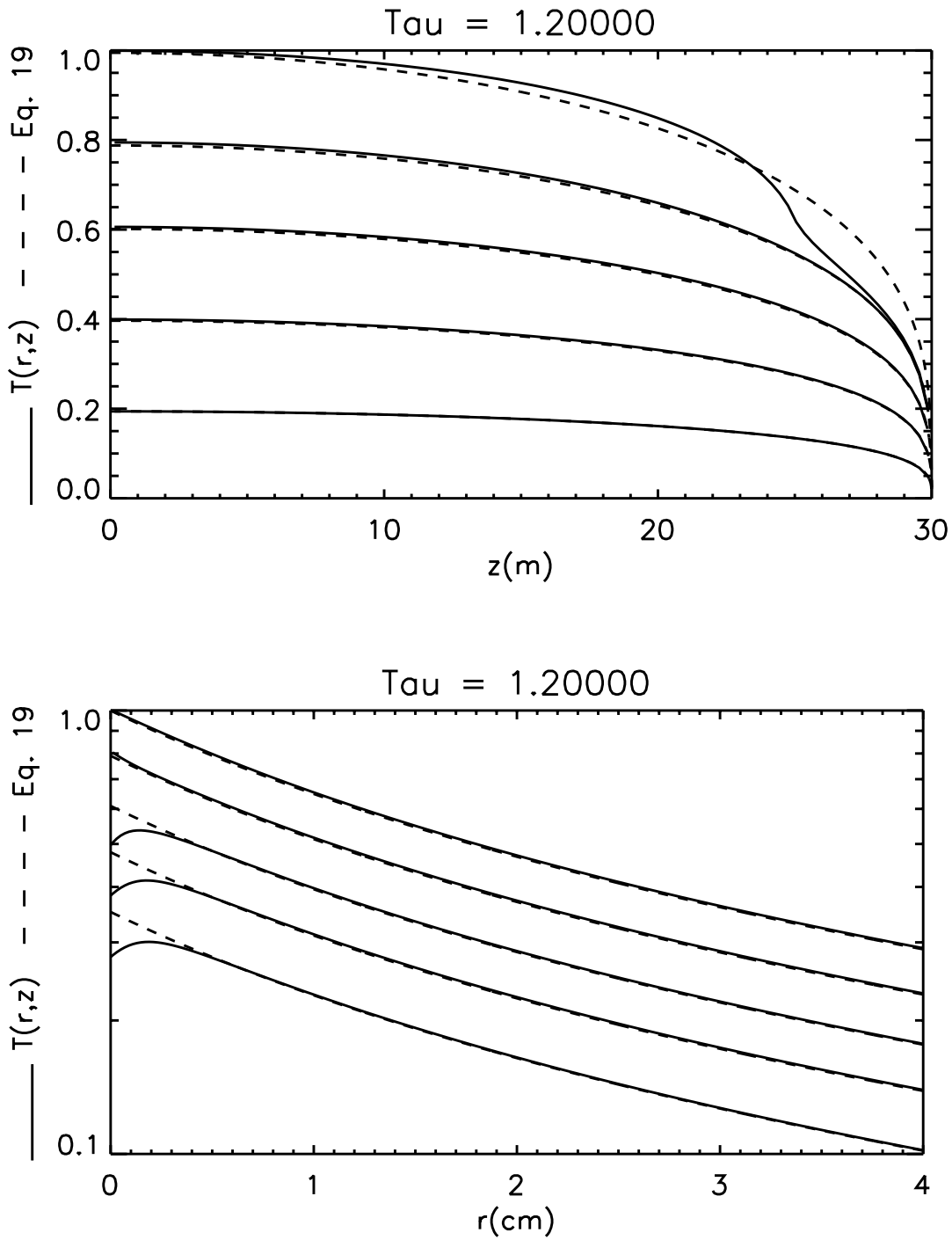


**Figure 7.** a) Numerical solution and self-similarity solution for  $T(z)$  with  $r = 0.01, 0.51, 1.21, 2.61, 6.31$  cm. Corresponds to conditions of figure 6b, Spitzer-scaling for parallel thermal diffusivity, Bohm for perpendicular.  $\tau = 1.2$ ,  $L_{\parallel}/\tau = 25$ m. b) Numerical solution and self-similarity solutions for  $T(r)$  with  $z = 0.15, 21.75, 26.85, 28.65, 29.55$ m.

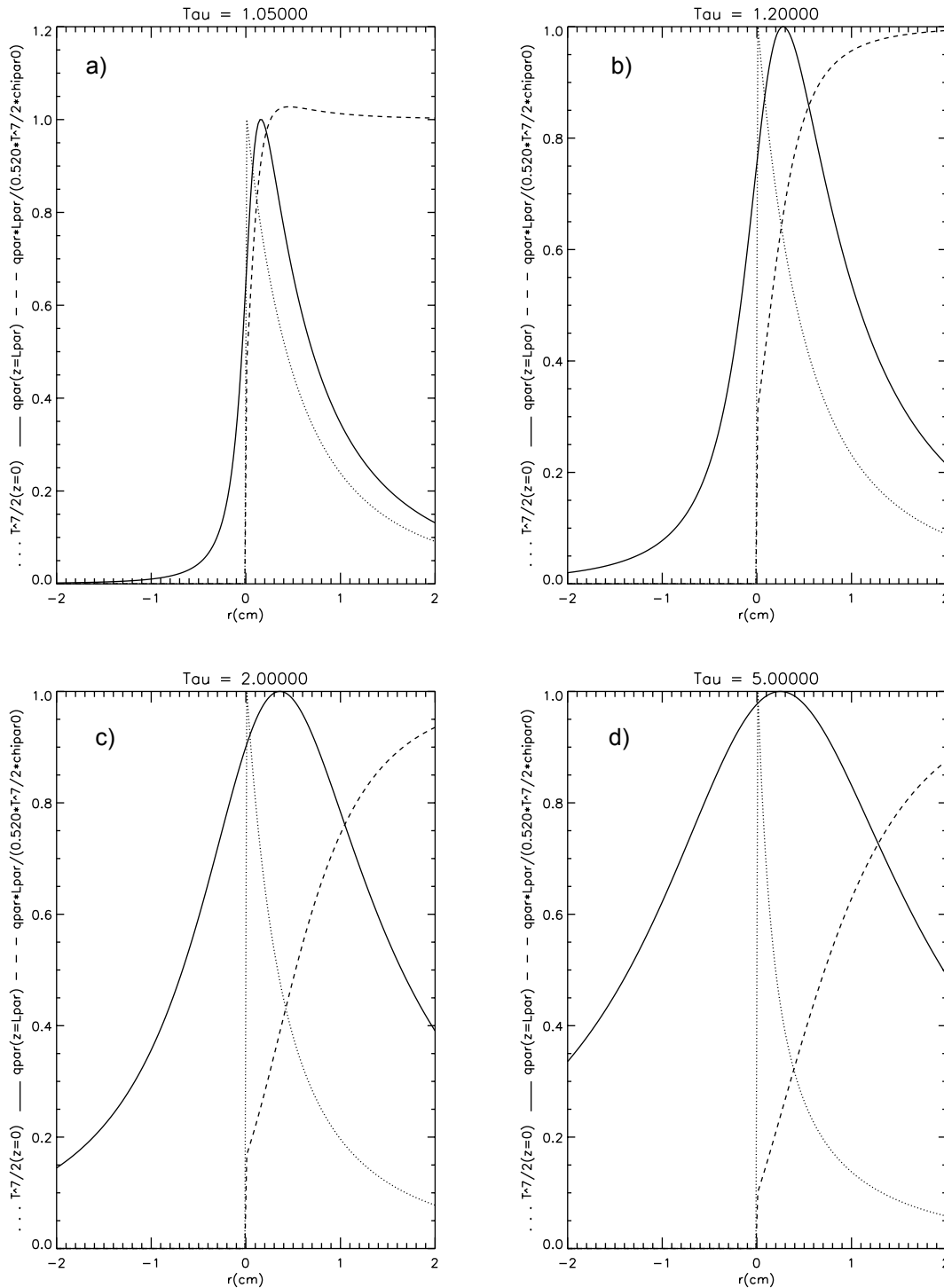


**Figure 8.**  $T^{7/2}(r)$  at  $z = 0$ ,  $q_{\parallel}(r)$  at  $z = L_{\parallel}$  and  $q_{\parallel}(r, z = L_{\parallel})L_{\parallel} / (0.520T^{7/2}(r, z = 0)\chi_{\perp 0})$ , ratio of divertor heat flux to midplane  $T^{7/2}$  normalized to expectation based on self-similarity solution, for various values of  $\tau$ . Numerical solution with Spitzer scaling of parallel thermal diffusivity, perpendicular thermal diffusivity given by  $\chi_{\perp} = 1m^2 / sec$  and boundary conditions of figure 2.

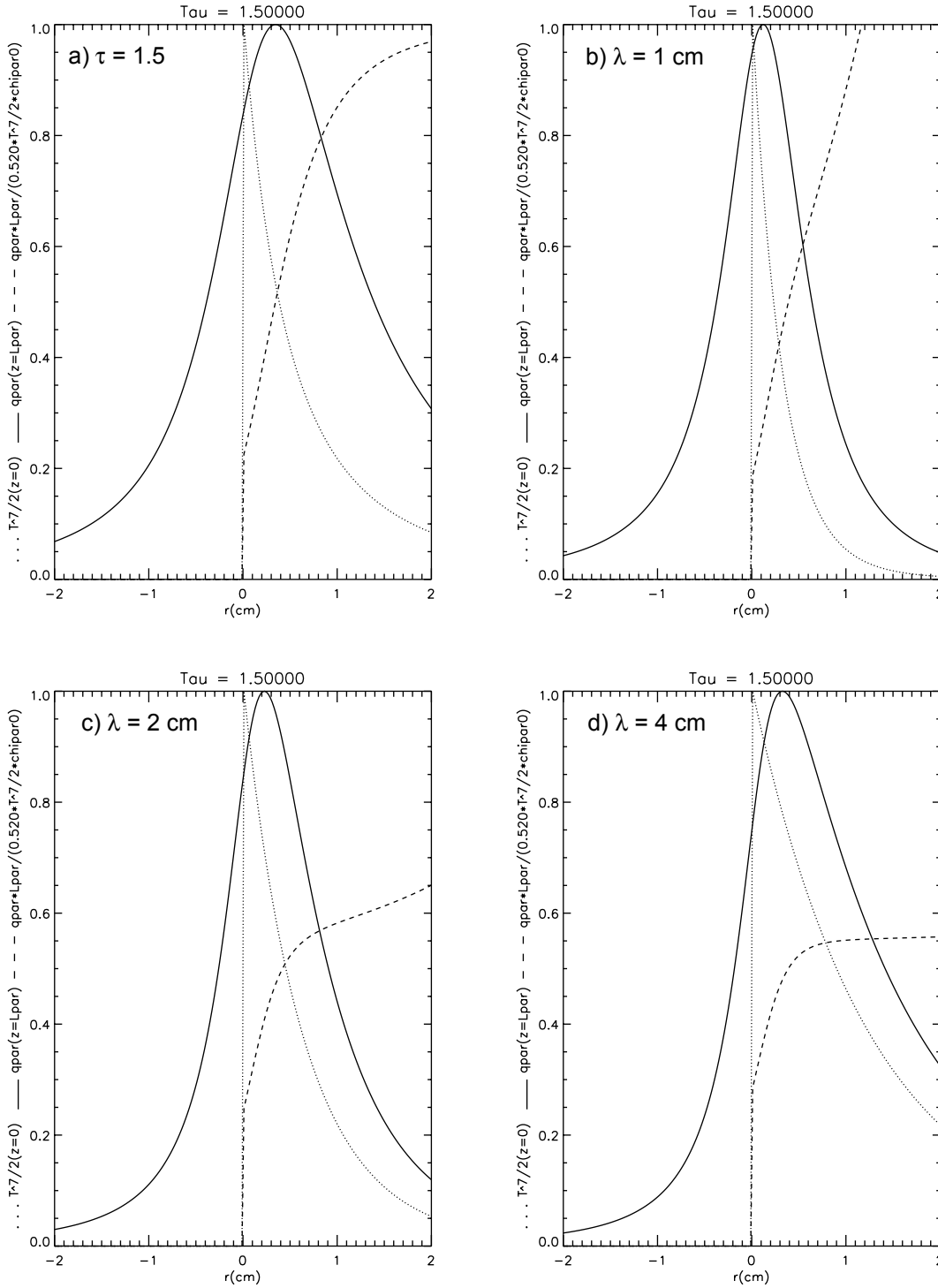


**Figure 9.** a) Same conditions as figure 7, for  $\tau = 1.5$ . b) – d) Same conditions as a), but with  $T(r)$  fixed exponential shape for  $|z| < L_{||}/\tau$ . Note that  $L_{||} = 10$ m for the dashed line, taking into account the fixed  $T(r)$  for  $|z| < 20$ m.

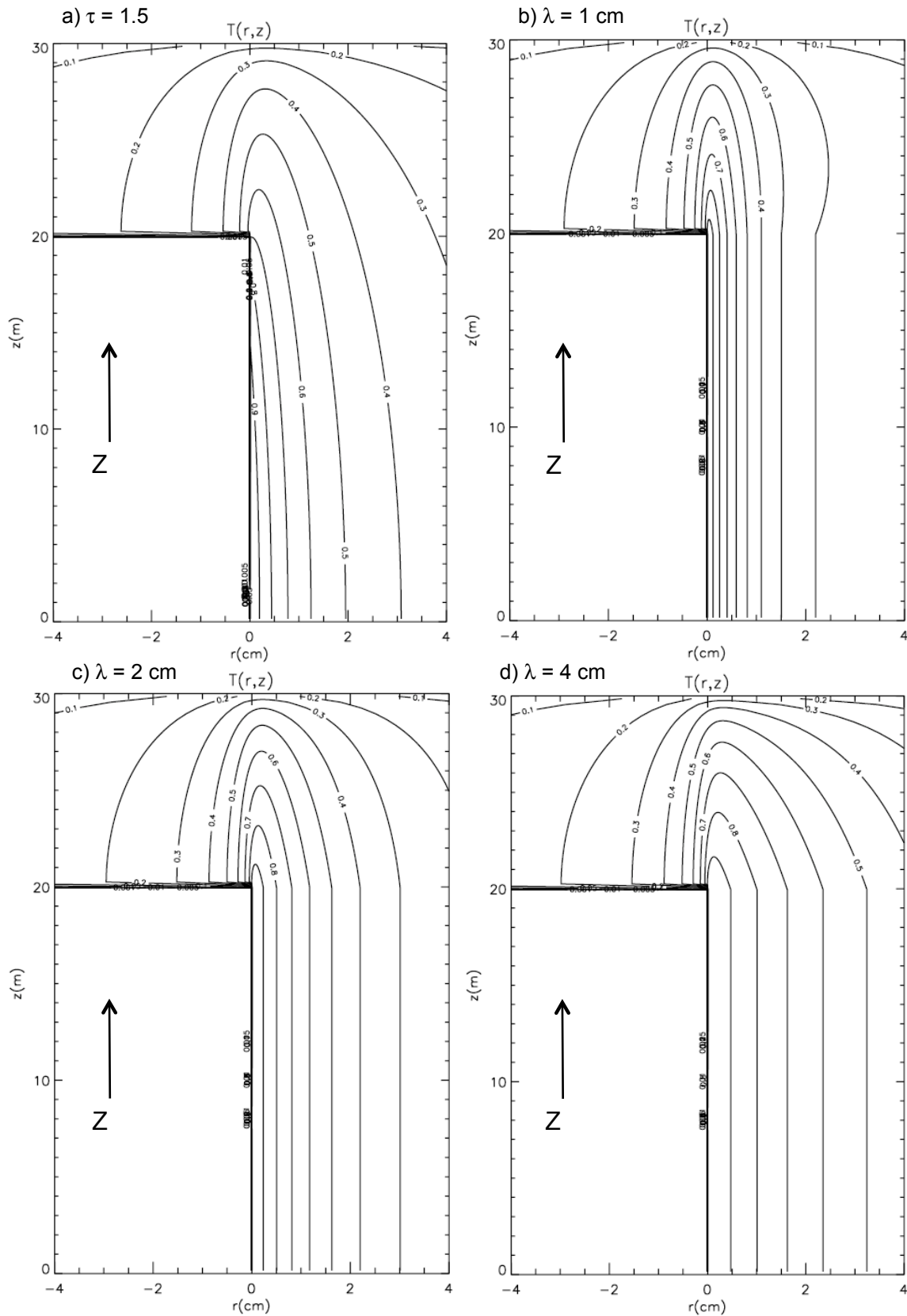


**Figure 10.** Contour plots of  $T$  for the cases shown in figure 8. Note that the geometry is flipped vertically compared with Figure 2.



The Princeton Plasma Physics Laboratory is operated  
by Princeton University under contract  
with the U.S. Department of Energy.

Information Services  
Princeton Plasma Physics Laboratory  
P.O. Box 451  
Princeton, NJ 08543

Phone: 609-243-2750  
Fax: 609-243-2751  
e-mail: [pppl\\_info@pppl.gov](mailto:pppl_info@pppl.gov)  
Internet Address: <http://www.pppl.gov>